Deep-Learning-Based Resource Allocation for Multi-Band Communications in CubeSat Networks

Shuai Nie*, Josep M. Jornet†, and Ian F. Akyildiz*
*Broadband Wireless Networking Lab, School of Electrical and Computer Engineering
Georgia Institute of Technology, USA
{shuainie, ian}@ece.gatech.edu
†Department of Electrical Engineering, University at Buffalo, The State University of New York, USA
jmjornet@buffalo.edu

***Abstract*—CubeSats, a type of miniaturized satellites with the benefits of low cost and short deployment cycle, are envisioned as a promising solution for future satellite communication networks. Currently, CubeSats communicate only with ground stations under limited spectrum resources and at low data rates, whereas with growing launches of CubeSats and more diverse services expected every year, novel communication techniques and resource allocation schemes should be investigated. In this paper, a multi-objective resource allocation strategy is designed based on deep learning algorithms for autonomous operation in CubeSats across millimeter wave (60–300 GHz) and Terahertz band (300 GHz–1 THz) frequencies with the utilization of reconfigurable plasmonic reflectarrays. Simulation results demonstrate the inter-satellite links can achieve multi-gigabits-per-second throughput and ground-to-satellite links with more than 10 times of capacity enhancements in realistic channel conditions.**

***Index Terms*—CubeSats, Satellite Communications, Millimeter wave, Terahertz band, Metasurfaces, Graphene, Deep Learning**

I. Introduction

In recent decades, the scope of the Internet of Things (IoT) has advanced in numerous vertical markets ranging from healthcare, cargo transportation, autonomous driving, among others. Existing IoT networks mainly rely on terrestrial cellular networks to accommodate enormous data traffic around the globe. New standards have been developed to address the ever-increasing demands of services and devices, for instance, the narrowband IoT [1]. Nonetheless, many constraints still impede the overall performance of the IoT, including extending services to places without infrastructure (either damaged or non-existent), combining a multitude of data types, including satellite imagery, asset tracking, and so on. For this, a new paradigm of IoT is necessary to tackle those problems.

With advantages in low cost and short production cycle, nano-satellites are burgeoning in commercial use of space such as Earth sensing, imaging, asset tracking, among others. Recent technical advancement in nano-satellites has attracted significant attention on their potentials to compose the *Internet of Space Things* (IoST), where the dimension of IoT is stretched to encompass the nano-satellites, aircraft, and spacecraft for connectivity. Among various configurations of nano-satellites, CubeSats, which were originally used for university education and research, have been deployed for services in low Earth orbit (LEO) including Earth remote sensing, weather forecasting, and machine-to-machine communication [2]. For instance, Planet Labs has launched a total of 175 CubeSats to support high-resolution Earth imaging services. CubeSats are also deployed in deep space for missions including interplanetary data relaying, sensing and monitoring on the Moon, Mars, and several asteroids, as well as even further in deep space. For example, the Mars Cube One (MarCO) mission from NASA consists of a pair of CubeSats aimed at the exploration of Mars. More promising CubeSat missions including interplanetary CubeSats will be enabled with future advancements in physics, electronics, and telecommunications [3].

The radio frequency (RF) bands utilized in conventional satellite communications include the L-band (1–2 GHz), S-band (2–4 GHz), C-band (4–8 GHz), X-band (8–12 GHz), Ku-band (12–18 GHz), K-band (18–27 GHz), and Ka-band (26.5–40 GHz). These frequency bands are being heavily utilized which can cause severe interference and thus degrade system performance. Therefore, with very limited bandwidth resources, existing CubeSats can only support very low data rates of up to a few kilobits-per-second, which set an extremely high delay and significantly impact the performance of satellite communication networks and, ultimately, would impact the performance of the IoST. Hence, innovative transceiver as well as antenna technologies should be investigated for new satellite link viabilities. Recently, NASA has initiated the development of an integrated solar reflectarray antennas operating at the Ka-band in CubeSats to push for downlink data rates to 100-Mbps [4]. Reflectarrays can be patched to the solar panels in CubeSats for easy folding. In parallel, the possibility to utilize the terahertz (THz) band for inter-satellite communication has been recently proposed [5]. THz-band frequencies offer the advantages of more abundant spectrum resource and a better tolerance of signal beam misalignment. We envision that future CubeSats should equip with the multi-band connectivity across microwave, millimeter wave, THz band, and optical frequencies, which requires new transceivers and antenna systems design. In this direction, we proposed our solution of a hybrid electronics-photonics-based transceiver design and the plasmic reflectarrays to realize reconfigurable antenna patterns [6].

To accommodate different levels of data link requests among

This work was supported by the U.S. National Science Foundation under Grant No. ECCS-1608579 and in part by Alexander von Humboldt Foundation through Ian Akyildiz's Humboldt Research Prize in Germany.

978-1-7281-2373-8/19/$31.00 ©2019 IEEE

end-users and multiple CubeSats, the diversity of available resources, including different frequency bands, distinct bandwidths, various antenna patterns, among others, makes resource allocation a very relevant challenge. Traditional approaches based on the use on-the-ground centralized decisions are not adequate because of the very long propagation delay associated to ground-to-satellite and satellite-to-satellite links. Similarly, preplanned resource allocation cannot cope with the dynamic communication needs of the IoST. Moreover, realistic satellite communication channel conditions require an adaptive solution to mitigate the significant Doppler shift and compensate the heavy rain fade.

In this paper, we develop and investigate the performance of a new resource allocation scheme based on deep learning algorithms especially suitable for dynamic system deployment. The contributions of this work are three-fold. First, we propose a multi-objective resource allocation scheme based on an ensemble deep neural network and, considering the limited energy and computation budget in CubeSats, instead of using classic backpropagation algorithm to calculate weight of each neuron, we utilitize random hill-climbing algorithm to adjust weights of neurons. Second, for the ground-to-satellite links, we examine the influence of Doppler shift due to movements of CubeSats and treat the factor as one of the features in our deep neural network. This enables CubeSats the capability to transmit and receive between others in different orbits, albeit the relatively high motions. Third, our design is based on the actual operational environment with real satellite trajectory data of the Iridium NEXT and simulate the satellite communication channel considering various atmospheric conditions.

The rest of the paper is organized as follows. In Sec. II, the main functioning components in CubeSats and its communication subsystem are introduced. In Sec. III, the dynamic resource allocation scheme based on deep learning algorithms is described. In Sec. IV, the numerical results based on simulation and performance analysis are given. Finally, the conclusion is drawn in Sec. V.

II. System Model

In the IoST, the CubeSats orbiting the Earth form a network in the *space segment*, while the links between the CubeSats and the ground stations define the *ground segment*, as shown in Fig. 1. In this section, we first describe the general architecture of CubeSats and then focus on our recently-proposed multi-band communication system in next generation CubeSats.

A. General Architecture of CubeSats

CubeSats have standardized sizes denoted as 1U, 2U, 3U, and so on, where a "U" means a $10\times10\times10$ cm^3 cube to fit the secondary payload slots in launch vehicles. The structure of a CubeSat follows specifications by NASA, the Joint Space Operations Center (JSpOC), and other space agencies worldwide. A CubeSat contains the following subsystems to maintain basic operations: i) an electrical power subsystem providing energy source; ii) a command and data handling subsystem which controls configurations; iii) an attitude determination and control subsystem managing positions of CubeSats and antenna pointing accuracy; iv) a payload subsystem carrying sensing and imaging devices such as cameras, spectrometers, telescopes, and so on; and v) a communication subsystem which transmits and receives data to and from ground stations and other CubeSats. A more detailed description of the CubeSat architecture can be found in [6].

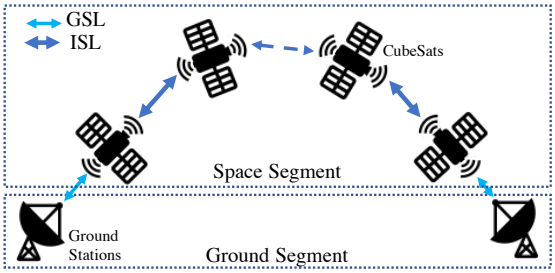

Fig. 1. A diagram of CubeSat links. The links between space and ground segment are ground-to-satellite links (GSLs) and the links among CubeSats are inter-satellite links (ISLs).

B. Multi-band Transceivers of CubeSats

Beside the aforementioned frequency bands deployed for conventional satellite communications in Sec. I, recently, free space optical (FSO) communication has also drawn notable attention as a candidate technique for CubeSat communications [3]. The FSO has the advantages of small aperture size and high throughput, but requires stringent beam matching at transceivers. On the other hand, millimeter wave (mm-wave) and terahertz (THz) band have less strict requirements on beam alignment and still offer abundant spectrum resources. In our proposed CubeSats, the communication subsystem will employ a multi-band communication subsystem with capabilities to dynamically allocate spectrum and power resources corresponding to specific channel conditions.

The communication subsystem is aimed to transmit and receive signals from ground stations, UAVs, and neighboring satellites, hence it incorporates multi-band transceivers and antenna arrays needed to support high-throughput inter-satellite and ground-satellite links from RF to THz to FSO. To fulfill the task, we have designed a hybrid integration of two complementary signal generation and modulation approaches, namely, an electronics-based approach and a photonics-based approach. In this paper, we focus on the design of algorithms which can dynamically change the operating frequency and transmit power as the resource allocation scheme of the multi-band communication subsystem of CubeSat. As for the process of multi-band signal generation, readers can refer to the details of this complimentary approach in [6].

C. Multi-band Reconfigurable Antenna Array

Plasmonic reflectarray antennas can efficiently radiate at the target resonant frequency while being much smaller than the corresponding wavelength [7], [8]. This peculiar character has allowed them to be integrated in very compact sizes, much denser than traditional antenna arrays. In our previous works,

TABLE I
ORBITAL AND COMMUNICATION LINK PARAMETERS (BASED ON THE IRIDIUM NEXT CONSTELLATION)

Notation	Parameter	Value Range
$n_s^{(k)}$	Number of CubeSats in the k-th orbit	11
K	Total number of orbits	6
$n_0^{(k,l)}$	Mean motion of the l-th CubeSat in the k-th orbit [Revolutions per day]	[14.33, 16.54]
$e_0^{(k,l)}$	Eccentricity	[0, 0.0241]
$E_0^{(k,l)}$	Eccentricity anomaly [deg]	[3.12, 356.74]
$i_0^{(k,l)}$	Inclination angle [deg]	86.4
$M_0^{(k,l)}$	Mean anomaly [deg]	[22.82, 345.27]
$\alpha_0^{(k,l)}$	Semi-major axis [km]	[6507.3, 7157.8]
$\iota_0^{(k,k',l)}$	Arc-length distance between two neighboring satellites in the same orbit [km]	[204.2, 230.8]
R	Rain rate [mm/hr]	[0.1, 16]
T	Temperature [Kelvin]	[290, 1500]
Γ_{min}	Minimum require link throughput [Mbps]	[0.512, 1.5]

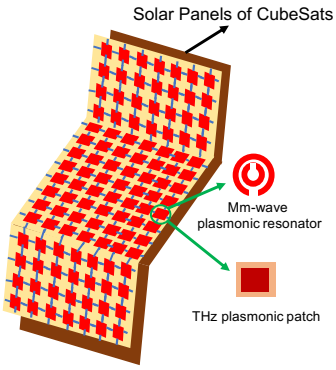

Fig. 2. A diagram of a multi-band reconfigurable antenna array which can be mounted on the back of CubeSats' extendable solar panels.

we have demonstrate that graphene can be used to build nano-antennas with maximum dimension $\lambda/20$, allowing them to be densely integrated in very small footprints (1024 elements in less than 1 mm^2) [7] and that graphene-based plasmonic nano-antenna arrays can enable multi-band communications with a suppressed mutual coupling effect [9]. However, graphene does not perform well at millimeter wave bands. Instead, we consider to incorporate metasurfaces into the plasmonic transmit-receive arrays. Metasurfaces, the 2D representation of metamaterials, have been well studied from the perspective of material science and technology [10].

To meet the size specification of CubeSats, the plasmonic reflectarrays can be deployed freely in the 3D environment, with a size ranging from 1 mm^2 to 100 mm^2 depending on the operating frequency (mm-wave/THz-band) equipped with hundreds or thousands of plasmonic antenna elements, as shown in Fig. 2. Owing to the sub-wavelength size of their elements, the plasmonic reflectarrays are able to reflect signals in non-conventional ways, which include controlled reflections in non-specular directions as well as reflections with polarization conversion [11]. In order to adapt to dynamic frequency operation in CubeSat links and allocate multiple beams to serve multiple sensing or data forwarding tasks, we can control the aperture of plasmonic reflectarray antenna through folding, splitting, or combining its subarrays. Hence, the directivity of plasmonic reflectarray antenna, can be expressed as a function of the tunable aperture, $D^{(k,l,x)} = 4\pi A_e^{(k,l,x)}/\lambda^2 \eta_e^{(k,l,x)}$, in which $(\cdot)^{(k,l,x)}$ represents the variable used by the l-th CubeSat in the k-th orbit for the x-th task. In later sections we also follow the same format to define orbital and link variables.

On the basis of multi-band signal generation, the multi-band communication system will utilize electronically-controlled frequency-tunable antenna arrays, by leveraging the tunability of plasmonic antennas. In particular, one of the relevant properties of graphene-based plasmonic nano-antennas is the possibility to change their resonant frequency by utilizing a small voltage to modify their Fermi energy [7]. The possibility to tune an antenna (or group of antennas) at different frequencies without any mechanical modification (as opposed to other multi-band antenna arrays that utilize MEMS or NEMS to create origami type structures [12]) enables beamforming not only across space but also across frequencies.

D. The Two-Line Element Orbital Data

In order to examine the feasibility for inter-satellite links, we need to accurately estimate the positions and mobility of CubeSats. In record of the trajectory information for Earth-orbiting objects, the two-line element (TLE) set is used for all current satellites and is available to public [13]. In TLE, the following key trajectory parameters can be extracted or derived based on simplified perturbation models and utilized as reference for our CubeSat design and simulation: epoch, eccentricities, inclinations, mean anomalies, mean motions, altitudes, velocities, among others, as shown in Table I. In our deep neural network, we derive link budget parameters and rely on these orbital statistics to determine the desired frequency bands and power levels for our proposed CubeSat communication links.

In our work, we collected the orbital data of the entire set of 66 Iridium NEXT satellites from the TLE dataset ranging from January 1 to 30, 2019, which corresponds to approximately 675,000 samples with eight input features. To calculate the inter-satellite arc-length distances for ISLs, we extract the mean anomaly M_0 and eccentricity e_0 to iteratively solve for the eccentricity anomaly E_0 within a small calculation error (i.e., e^{-10}) based on the Kepler's equation $M_0 = E_0 - e_0 \sin E_0$. Then by assuming the same orbit

speed v, we can calculate the arc-length distance between two satellites based on their respective times to the periapsis as

$$\begin{aligned}\iota &= v\left[(t_1 - t_p) - (t_2 - t_p)\right] \\ &= v\sqrt{\frac{\alpha_0^3}{\mu}}\left[(E_1 - e_1 \sin E_1) - (E_2 - e_2 \sin E_2)\right],\end{aligned} \tag{1}$$

in which μ is the standard gravitational parameter for the Earth and α_0 is the semi-major axis for the orbit.

III. Multi-Band Communication and Resource Allocation Scheme

While CubeSats perform sensing and monitoring tasks, the data generated should be efficiently transmitted to ground stations and task commands should be received with minimum delay. The goal of multi-band communication for CubeSat networks is to maximize the link throughput, minimize the delay, and mitigate any possible interference from other links. However, several environment factors should be characterized, including rain fading and fast Doppler shift.

A. Influence of Weather on CubeSat Multi-Band Links

In satellite communication scenarios, space and atmospheric weather has non-negligible effects on the survivability of GSLs [14]. Among them, rain fading plays a crucial role. According to the ITU's recommendation, it is demonstrated that the rain attenuation is a function of the communication frequency f_c, rain rate R, and two polarization-specific coefficients, k and α, which form a relationship as follows,

$$\begin{aligned}\log \gamma_R &= \log k + \alpha \log R, \\ &= \sum_{j=1}^{4}\left(a_j \exp\left[-\left(\frac{\log f_c - b_j}{c_j}\right)^2\right]\right) + m_k \log f_c \\ &+ c_k + \log R\left[\sum_{j=1}^{5}\left(a_j \exp\left[-\left(\frac{\log f_c - b_j}{c_j}\right)^2\right]\right)\right. \\ &\left. + m_\alpha \log f_c + c_\alpha\right],\end{aligned} \tag{2}$$

in which a_j, b_j, c_j, m_k, and c_k are coefficients dependent on frequency and polarization conditions [15]. We can hence accurately capture the attenuation caused by the water molecules at frequencies up to 1 THz in GSLs. When a ground station needs to connect to a CubeSat or vice versa, the power budget takes into account the rain fade at the intended frequency.

B. Influence of Doppler Shifts on CubeSat Multi-Band Links

Unlike most terrestrial communication scenarios, satellites are in constant orbital movements. Even though we can treat the arc-length distance between two adjacent CubeSats in the same orbit as an approximately stable value, the Doppler effect in GSLs cannot be neglected. When the beacon signals at frequency sent from a CubeSat received by the ground station, the receiver should determine if it needs to connect to this CubeSat the as a prograde movement leads to a higher receiving frequency and a retrograde movement leads to a lower one, based on the measured Doppler frequency f_D, such that we have a channel with coherence time T_c as

$$\arg\max_{f_D} T_c(f_D) = \left\{ f_D \mid \frac{9}{16\pi f_D} \le T_c \le \sqrt{\frac{9}{16\pi f_D^2}} \right\}. \tag{3}$$

Hence, in our GSL modeling, we also take into account the adaptive Doppler shift compensation in the spectrum resource allocation scheme.

C. Multi-Objective Optimization Problem Formulation

We consider a four-tuple parameter set for resource allocation, which includes the transmit power P_t, the bandwidth W_b, the center frequency f_c, and the directivity of plasmonic reflectarray antennas D_t. We can formulate an optimization problem in the following form,

$$\begin{aligned}\textit{Given: } & n_s^{(k)}, K, n_0^{(k,l)}, e_0^{(k,l)}, i_0^{(k,l)}, M_0^{(k,l)}, \alpha_0^{(k,l)}, \\ & \Gamma_{\min}^{(x)}, \mathrm{BER}_{\min}^{(x)}, P_{\mathrm{res}}^{(k,l)}, \mathbf{f}_c, \mathbf{W}_b, \gamma_R. \end{aligned} \tag{4}$$

$$\textit{Find: } P_t^{(k,l,x)}, f_c^{(k,l,x)}, W_b^{(k,l,x)}, D^{(k,l,x)}. \tag{5}$$

$$\begin{aligned}\textit{Objectives: } & \max \sum \Gamma^{(k,l,x)}, \min \sum P_r^{(k,\bar{k})}, \\ & \min \sum \tau^{(x)}. \end{aligned} \tag{6}$$

$$\textit{Subject to: } \sum P_t^{(k,l,x)} \le P_t^{\mathrm{tot}} \text{ (Transmit power allocation)}, \tag{7}$$

$$\sum n_s^{(k,l,x)} \le N_s^{\mathrm{tot}} \text{ (CubeSat allocation)}, \tag{8}$$

$$\sum D^{(k,l,x)} \le D^{(k,l)} \text{ (Antenna array allocation)}, \tag{9}$$

$$\begin{aligned}& \Gamma\left(P_t^{(k,l,x)}, n_s^{(k,l,x)}, D^{(k,l,x)}\right) \ge \Gamma_{\min}^{(x)}, \\ & \forall k \in K \text{ and } \forall l \in L_{orb}. \end{aligned} \tag{10}$$

We can observe that this problem is a combinatorial optimization problem which cannot be easily solved. Therefore, we seek help from machine learning techniques which have recently burgeoned for communication network use cases.

D. Resource Allocation Optimization via DNN

In the field of machine learning, deep learning has recently gained significantly promising results in tackling complicated wireless network problems with large data volumes [16]. It is fair to believe that future wireless communication networks will be more intelligent with the utilization of deep learning techniques. In the space network, we also face the challenges of handling, processing, and transmitting sheer amount of data amongst CubeSats and ground stations in complicated space channels. Lacking real-time knowledge of CubeSat orbital conditions and only having centralized control stations on the Earth will not only hinder prompt data handling, but also often yield undesirable end-to-end throughput. The resource allocation scheme is resulted from a deep neural network (DNN) that aims to optimize the frequency bands, transmitted power levels, as well as adjust the radiation patterns of

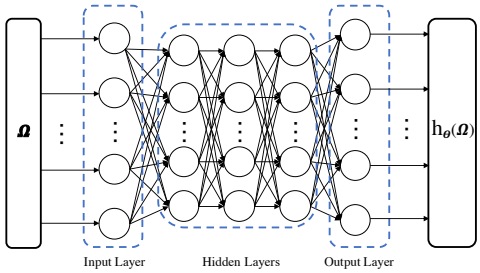

Fig. 3. Architecture of the deep neural network for CubeSat links. Five layers of neurons are connected to process the input feature space Ω.

reconfigurable antenna arrays. Since the optimization targets are independent of each other, we can train an ensemble deep neural network with each finding the global optimum of the specific goal.

In classic DNN architectures, each neuron connected through multiple layers has a certain associated weight which is determined by the algorithm called backpropagation [17]. Backpropagation relies on calculating the gradient of the loss function in order to adjust the initial weights of neurons, which has been proved to be an efficient solution to find the global optima. However, in scenarios where computation complexity and energy consumption become major constraints in employing backpropagtion for finding optimal weights, other efficient yet less energy-draining methods should be considered. In particular, randomized optimization algorithms are preferable candidates in the CubeSat communication network.

Random hill-climbing (RHC) algorithm finds the "peak" value among all values in the "landscape" by comparing the current value with the one in previous step. It has the advantages of low memory requirement as well as low time complexity, compared to neural networks with backpropagation and other optimization methods including the genetic algorithm and simulated annealing. The initial step is randomly chosen. Then a modification is made in the next step and comparison is performed with the previous one: if current step yields a better solution, then we accept it as the temporary solution, and continue moving along the same direction as well as making comparison with next steps; if current step does not outperform the previous one, then we discard it and suggest a new value, or "restart" the research for the local optimal solution. After some iterations, the number of which is predetermined, or the improvement is not significant, the algorithm will stop.

In the CubeSat network, with the intrinsic characteristics of limited power and on-board memory budget, we apply random hill climbing algorithm in the DNN in place of the backpropagation. In our DNN, as shown in Fig. 3, we first construct the input feature space Ω, which is a matrix with the following quantized column vectors based on the real orbital data from the Iridium,

$$\mathbf{\Omega} = [\iota, \gamma_R, f_D, T, \Gamma_{min}, \text{BER}_{min}, f_c^{(all)}, W_b^{(all)}]^\intercal. \quad (11)$$

We then employ the sigmoid function as the activation function in this DNN, which is expressed as $h_\theta(\mathbf{\Omega}) = \frac{1}{1+\exp(-\theta^\intercal \mathbf{\Omega})}$.

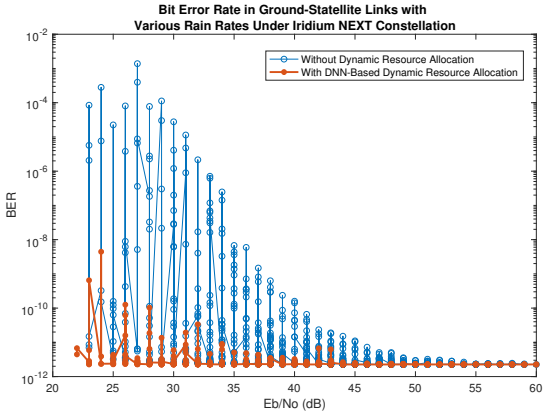

Fig. 4. BER performance in GSLs at different rain fading scenarios.

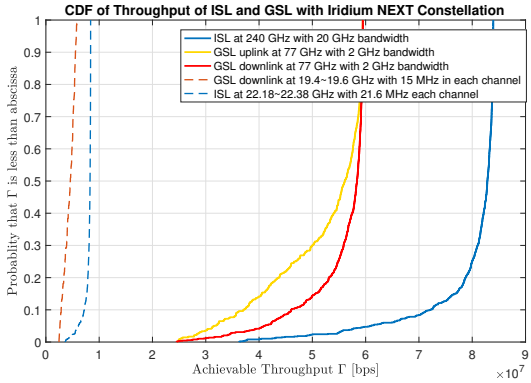

Fig. 5. Comparison of the CDF of throughput with existing Iridium NEXT frequencies and proposed mm-wave/THz dynamic resource allocation scheme.

We then construct a multi-class classification output as $\mathbf{y} = h_\theta(\mathbf{\Omega}) \in \mathbb{R}^S$, in which S is the size of the output units, or the number of classes. The output units are column vectors each with all elements to be 0 except one element has a value of "1" indicating the classified output. In each deep neural network in our ensemble structure, we have four layers, and the number of hidden neurons in the layers are $[75, 50, 30, 12, 6]$. The output is corresponding to the indicator value which points to the selected frequency bands, transmitted power level, and values of directivity of antenna array. In the training data, we split the training dataset into 80% and 20% as the training and the validation set to perform cross-validation on the weights. The numerical results on link performance based on the selected parameters are drawn in the following section.

In the perspective of actual deployment, recent advancements have been made available in industry to ensure ultra-low power consumption and miniaturized size for neural computation hardware. For example, the Movidius technology developed by Intel is the miniaturized neural compute engine which can ignite the future deployment of deep neural network at very low power consumption, implying a good fit for low power budget in CubeSats.

IV. Results and Analysis

Based on the DNN we constructed and trained with inputs based on the real orbital data from Iridium NEXT constel-

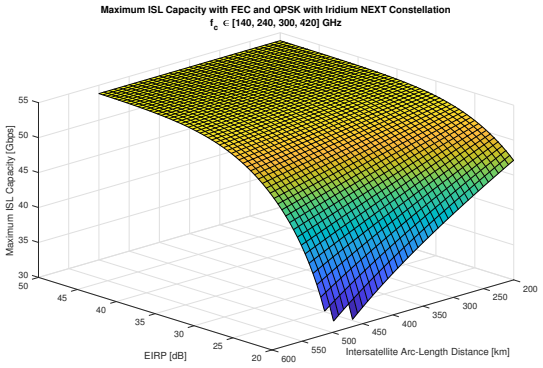

Fig. 6. The maximum achievable throughput in ISLs at various inter-satellite distances with EIRP and frequency optimization.

lation, we can perform testing using the connected neurons with weights found by random hill-climbing technique. In our simulated satellite communication scenarios, a pair of fixed end-users are on the ground with two locations on the east and west hemisphere and hence rely on the satellite network for communications. Therefore in the end-to-end link path which consists of a GSL uplink, multiple ISLs, and a GSL downlink, we compare the performance in terms of i) bit error rates (BERs) given selected values of transmitted power and antenna array gain (i.e., directivity), ii) the achievable throughput values with various link distance (e.g., the arc-length distance in ISLs and line-of-sight distance in GSLs), and iii) the maximum throughput CubeSat network can achieve by using the dynamic resource allocation scheme in ISLs.

In both the GSL and ISL data links, we apply the forward error correction with the $BCH(63, 39, 4)$ coding scheme and QPSK is used as the modulation scheme. We send a packet with a total length of 1500 bytes. According to the Iridium NEXT constellation, the frequency bands for ISL spans eight channels in 22.18–22.38 GHz, each with a 21.6 MHz bandwidth, the feeder uplink has 13 channels in 29.1–29.3 GHz and downlink has 13 channels in 19.4–19.6 GHz, each with approximately 15.3 MHz bandwidth. In our proposed CubeSat links, the candidate frequency bands for ISL include 60, 140, 240, 300, and 420 GHz and for GSL 77 and 120 GHz. As shown in Fig. 4, various rain rates cause different level of link degradation without applying dynamic resource allocation. Each sample represents an actual GSL with a longitude ranging near poles (with the best BER) and equator (with the lowest BER). Using dynamic bandwidth and transmit power allocation, the BER performance near the equator improves significantly.

The comparison of ISLs and GSLs at K-band and higher frequencies is drawn in Fig. 5. The achievable throughput of Iridium NEXT in ISLs matches with the engineering statement by Iridium [18], while the proposal frequencies at 77 and 240 GHz demonstrate at least ten times enhancement in throughput. The multi-Gbps links can be realized with the DNN-based resource allocation optimization scheme at various ISL frequencies, as shown in Fig. 6.

V. Conclusion

This paper presents the design of a multi-objective resource allocation scheme for CubeSat networks, which takes consideration of dynamic channel variations and aims to achieve optimal throughput in both GSLs and ISLs at multiple bands ranging from the microwave to the mm-wave and the THz band. Moreover, training of the real orbital data based on the Iridium NEXT constellation, the deep neural network-based resource allocation scheme is implemented with efficient random hill-climbing algorithm to fit the low power and computation budget of CubeSats. Simulation results show that the proposed scheme can help CubeSats to achieve multi-Gbps throughput in ISLs in the low Earth orbits.

References

[1] Y.-P. E. Wang *et al.*, "A primer on 3gpp narrowband internet of things," *IEEE Communications Magazine*, vol. 55, no. 3, pp. 117–123, 2017.

[2] I. F. Akyildiz and A. Kak, "The Internet of Space Things/CubeSats: A ubiquitous cyber-physical system for the connected world," *Computer Networks*, vol. 150, pp. 134–149, 2019.

[3] R. Staehle *et al.*, "Interplanetary cubesats: opening the solar system to a broad community at lower cost," *Journal of small satellites*, vol. 2, no. 1, pp. 161–186, 2013.

[4] D. Lewis, "Integrated Solar Array and Reflectarray Antenna for High Bandwidth CubeSats," https://ntrs.nasa.gov/archive/nasa/casi.ntrs.nasa.gov/20170009849.pdf, 2015.

[5] I. Mehdi, J. Siles, C. P. Chen, and J. M. Jornet, "Thz technology for space communications," in *2018 Asia-Pacific Microwave Conference (APMC)*, Nov 2018, pp. 76–78.

[6] I. F. Akyildiz *et al.*, "A new cubesat design with reconfigurable multi-band radios for dynamic spectrum satellite communication networks," *Ad Hoc Networks*, vol. 86, pp. 166 – 178, 2019.

[7] J. M. Jornet and I. F. Akyildiz, "Graphene-based plasmonic nano-antenna for terahertz band communication in nanonetworks," *IEEE JSAC, Special Issue on Emerging Technologies for Communications*, vol. 12, no. 12, pp. 685–694, Dec. 2013.

[8] M. Tamagnone, J. Gomez-Diaz, J. Mosig, and J. Perruisseau-Carrier, "Analysis and design of terahertz antennas based on plasmonic resonant graphene sheets," *Journal of Applied Physics*, vol. 112, no. 11, p. 114915, 2012.

[9] B. Zhang *et al.*, "Graphene-based frequency selective surface decoupling structure for ultra-dense multi-band plasmonic nano-antenna arrays," in *Proceedings of the 5th ACM NANOCOM*, 2018, pp. 27:1–27:6.

[10] M. J. Lockyear, A. P. Hibbins, and J. R. Sambles, "Microwave surface-plasmon-like modes on thin metamaterials," *Physical review letters*, vol. 102, no. 7, p. 073901, 2009.

[11] H. Zhu, S. Cheung, K. L. Chung, and T. I. Yuk, "Linear-to-circular polarization conversion using metasurface," *IEEE Transactions on Antennas and Propagation*, vol. 61, no. 9, pp. 4615–4623, 2013.

[12] S. Yao *et al.*, "A novel reconfigurable origami spring antenna," in *Antennas and Propagation Society International Symposium (APSURSI), 2014 IEEE*. IEEE, 2014, pp. 374–375.

[13] NORAD, "Current Space Track NORAD Two-Line Element Sets," https://www.celestrak.com/SpaceTrack/, January 2019.

[14] T. Tjelta *et al.*, "Results of a ka band campaign for the characterisation of propagation conditions for satcom systems at high latitudes," in *2017 11th European Conference on Antennas and Propagation (EUCAP)*, March 2017, pp. 1481–1485.

[15] ITU-T, "Specific attenuation model for rain for use in prediction methods," International Telecommunication Union, Recommendation P.838-3, March 2005.

[16] S. Dörner *et al.*, "Deep learning based communication over the air," *IEEE Journal of Selected Topics in Signal Processing*, vol. 12, no. 1, pp. 132–143, 2018.

[17] I. Goodfellow, Y. Bengio, A. Courville, and Y. Bengio, *Deep learning*. MIT press Cambridge, 2016, vol. 1.

[18] Federal Communications Commission, "Iridium NEXT Engineering Statement (Appendix to application to modify existing license)," August 2016.